

Impact of the PDFs on the Z and W lineshapes at LHC

Valerio Bertacchi¹, Elisabetta Manca, Gigi Rolandi, Suvankar Roy Chowdhury
Scuola Normale Superiore and INFN sezione di Pisa, Italy

Lorenzo Bianchini
INFN sezione di Pisa, Italy

Abstract

The parton distribution functions (PDFs) of the proton play a role in determining the lineshape of W and Z bosons produced at the LHC. In particular, the mode of distribution of the gauge boson virtuality gets shifted with respect to the boson mass due to the dependence of the partonic luminosity on the boson virtuality itself. This shift contributes to the systematic uncertainty on the direct measurement of the boson mass. A detailed study of the shift and of its systematic uncertainty due to the limited knowledge of the PDFs is obtained using a tree-level model of W and Z boson production in proton-proton collisions at $\sqrt{s} = 13$ TeV. For the special case of W boson production, a Monte Carlo simulation is further used to validate the tree-level model and study the dependence of the shift on the transverse momentum of the W boson. The tree-level calculation is found to provide already a good description of the shift. The systematic uncertainty due to the PDFs is estimated to be below one MeV in the phase-space relevant for a future high-precision measurement of the W and Z boson masses at the LHC.

arXiv:1909.07935v1 [hep-ex] 17 Sep 2019

¹Corresponding author, email: valerio.bertacchi@pi.infn.it

1 Introduction

The Drell-Yan production of massive lepton-pairs in hadron collisions [1] has been extensively studied in the literature both as a probe of the proton structure [2] and as a tool for precise electroweak measurements. In recent years, large efforts have been spent on understanding the role of the collinear parton density functions (PDFs) in the determination of differential distributions of leptonic variables sensitive to electroweak parameters, such as asymmetries in Z/γ production [3–5] and transverse observables in W events [6–8].

The unprecedented amount of W and Z bosons produced at the CERN Large Hadron Collider (LHC)² offers new opportunities on the critical path towards precision, but it also forces to consider sources of systematic uncertainty which may have been legitimately neglected so far, for example those related to the modeling of the virtuality of the gauge bosons [9]. For instance by analyzing the over 10^8 dileptonic Z decays which should become available by the end Run 3 of the LHC, a statistical-only precision of about $2 \text{ GeV}/\sqrt{10^8} \sim 10^{-5} \text{ GeV}$ on M_Z might be achievable, at least in principle. This level of precision would demand a control of the dilepton mass lineshape at the sub-MeV level.

At the lowest order in perturbation theory, the distribution of the virtuality Q of a gauge boson V produced at a given value of rapidity y , originates by the convolution of a relativistic Breit-Wigner with the the partonic luminosity function [10]. The latter is a function of the dimensionless parameter $\tau = Q^2/s$, where s is the square of the proton-proton center-of-mass energy. The non-trivial dependence of the partonic luminosity on τ implies a distortion of the lineshape compared to a pure Breit-Wigner. Given the narrowness of the electroweak gauge bosons width Γ_V , this effect can be treated, in first approximation, as a shift Δ_V of the mode of the distribution compared to M_V . The limited knowledge of the PDFs introduces an uncertainty on Δ_V , which contributes directly to the model uncertainty in the extraction of M_V from the dilepton mass distribution. The purpose of this work is to assess the size of this shift and of its PDF uncertainty in sight of a future high-precision measurement at the LHC.

This paper is organized as follows. In Sec. 2 a tree-level calculation of the shift Δ_V is presented. In Sec. 3, a Monte Carlo (MC) simulation of charged-current Drell-Yan production is used to validate the tree-level model and extend the study to the full phase-space of W production. The results are summarized in Sec. 4.

2 Tree level study

It is first considered a simplified model of Drell-Yan production based on a minimal subset of tree-level diagrams. This approximation amounts to consider just one Feynman diagram per quark-antiquark pair, as illustrated in Fig. 1(a) for the case of W production. Besides accounting already for the bulk of the total cross section (about 80% for a 20 GeV threshold on the transverse momentum of the extra parton at $\sqrt{s} = 13 \text{ TeV}$), these diagrams are also expected to be the most sensitive to the PDF-dependent shift that it would be determined. Indeed, they are the only $2 \rightarrow 1$ diagrams contributing to the amplitude, whereas higher-order diagrams are at least $2 \rightarrow 2$, see e.g. Fig. 1(b). As such, they include additional invariants besides Q . It is expected the existence of these extra scales to dilute the sensitivity of the lineshape on the details of the PDFs. This assumption will be validated by a MC analysis of $pp \rightarrow W^\pm + X$ production discussed later in Sec. 3. In the following, it will be used the NNPDF3.0 [2] set to evaluate the

²The CMS and ATLAS experiment collected order of 400 millions of W and 40 millions of Z bosons each during the Run 2 of LHC.

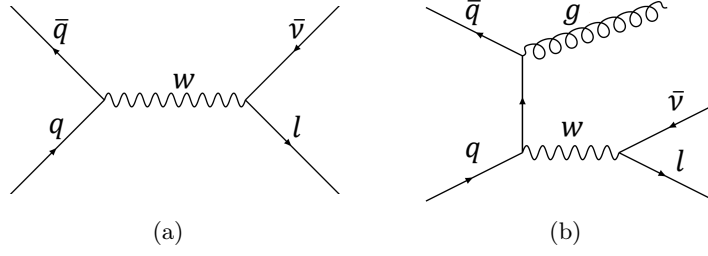


Figure 1: Tree level diagram (1(a)) and example of NLO diagram (1(b)) for W boson production.

PDFs relevant for W and Z production in proton-proton collisions at $\sqrt{s} = 13$ TeV.

Within the tree-level approximation, the double-differential cross section for $pp \rightarrow V(\rightarrow \ell\ell') + X$, as a function of the quark momentum fractions $x_{1,2}$, is given by

$$\frac{d^2\sigma_V}{dx_1 dx_2} = \frac{1}{N_C} \sum_{ij} [f_i(x_1)f_j(x_2) + f_i(x_2)f_j(x_1)] \frac{16\pi\Gamma_V^2 \text{BR}_{V \rightarrow q_i \bar{q}_j} \text{BR}_{V \rightarrow \ell\ell'}}{(x_1 x_2 s - M_V^2)^2 + M_V^2 \Gamma_V^2}, \quad (1)$$

where N_C is the number of QCD colours, M_V and Γ_V are the mass and width of the resonance, $\text{BR}_{V \rightarrow ab}$ are the relevant branching fractions, and the sum at the right-hand side runs over the different combinations of quark flavours contributing to the process under study. For simplicity, the scale-dependence is omitted from the quark PDF $f_i(x)$. In Eq. (1) a relativistic Breit-Wigner function with fixed width has been assumed, which is also the functional form used for the Monte Carlo simulation discussed in Sec. 3. Since the studied feature in Eq. (1) concerns the core of the distribution, where $Q \sim M_V$, the results would not change if a running-width scheme were assumed, the two schemes differing only when $|Q - M_V| \gg \Gamma_V$ [11].

In order to express the double-differential distribution Eq. (1) as a function of Q and y the canonical change of variables is performed:

$$y = \frac{1}{2} \ln \frac{x_1}{x_2}, \quad Q^2 = x_1 x_2 s. \quad (2)$$

By combining Eq. (1) and (2), it is obtained the single-differential distribution $d\sigma/dQ$, conditional on y :

$$\begin{aligned} \frac{d\sigma_V}{dQ}(Q | y) &= \left(\frac{d\sigma_V}{dy}\right)^{-1} \frac{1}{N_C} \sum_{ij} \frac{8Q}{s} [f_i(\bar{x}_1)f_j(\bar{x}_2) + f_i(\bar{x}_2)f_j(\bar{x}_1)] \frac{16\pi\Gamma_V^2 \text{BR}_{V \rightarrow q_i \bar{q}_j} \text{BR}_{V \rightarrow \ell\ell'}}{(Q^2 - M_V^2)^2 + M_V^2 \Gamma_V^2} \\ &\equiv \sum_{ij} C_{ij}^V [f_i(\bar{x}_1)f_j(\bar{x}_2) + f_i(\bar{x}_2)f_j(\bar{x}_1)] \frac{Q}{(Q^2 - M_V^2)^2 + M_V^2 \Gamma_V^2}, \end{aligned} \quad (3)$$

where $\bar{x}_{1,2} = \sqrt{\tau} e^{\pm y}$ and the constants C_{ij}^V include terms that depend on y but not on Q . The fact that $\Gamma_V/M_V \ll 1$ and that f_i are smooth functions in the relevant range of Bjorken x values ($10^{-3} \lesssim x \lesssim 10^{-1}$) can be exploited to perform a Taylor expansion of the right-hand side of Eq. (3) around $Q = M_V$:

$$\begin{aligned} \frac{d\sigma_V}{dQ}(Q | y) &\sim \frac{Q}{(Q^2 - M_V^2)^2 + M_V^2 \Gamma_V^2} \sum_{ij} |V_{ij}|^2 (F^{ij} + F^{ji}) \times \\ &\left[1 + \underbrace{\frac{\sum_{ij} |V_{ij}|^2 (F^{ij} H^{ij} + F^{ji} H^{ji})}{\sum_{ij} |V_{ij}|^2 (F^{ij} + F^{ji})}}_{H_V} \left(\frac{Q}{M_V} - 1\right) + \underbrace{\frac{\sum_{ij} |V_{ij}|^2 (F^{ij} K^{ij} + F^{ji} K^{ji})}{\sum_{ij} |V_{ij}|^2 (F^{ij} + F^{ji})}}_{K_V} \left(\frac{Q}{M_V} - 1\right)^2 \right] \end{aligned} \quad (4)$$

where the flavour-dependent terms have been factored out of $\text{BR}_{V \rightarrow q_i \bar{q}_j}$ in the form of the square of the V matrix elements. The latter should be interpreted as the usual CKM matrix for the case of W production, and as $(T_i^3 - 2Q_i \sin^2 \theta_W) \delta_{ij}$ for Z production, where T_i^3 and Q_i are the weak isospin and electric charge of quark i , respectively. In Eq. (4), the following auxiliary functions have been introduced:

$$\begin{aligned} F^{ij} &= [f_i(\bar{x}_1) f_j(\bar{x}_2)]_{Q=M_V} \\ H^{ij} &= \left[\frac{f'_i(\bar{x}_1)}{f_i(\bar{x}_1)} \bar{x}_1 + \frac{f'_j(\bar{x}_2)}{f_j(\bar{x}_2)} \bar{x}_2 \right]_{Q=M_V} \\ K^{ij} &= \frac{1}{2} \left[\frac{f''_i(\bar{x}_1)}{f_i(\bar{x}_1)} \bar{x}_1^2 + \frac{f''_j(\bar{x}_2)}{f_j(\bar{x}_2)} \bar{x}_2^2 + 2\bar{x}_1 \bar{x}_2 \frac{f'_i(\bar{x}_1) f'_j(\bar{x}_2)}{f_i(\bar{x}_1) f_j(\bar{x}_2)} \right]_{Q=M_V} \end{aligned} \quad (5)$$

where f' (f'') are the first (second) order derivative of the PDF with respect to x . The constants H_V and K_V defined in Eq. (4) represent the appropriate average of the auxiliary functions of Eq. (5) over the flavour space. The validity of the Taylor expansion of Eq. (4) has been assessed by comparing the lineshape from Eq. (3) and (4) at different values of y : the relative difference between the two is found to be below 0.5% for $Q \in [79, 82]$ GeV.

In Eq. (4), the contribution of the PDFs to the lineshape is fully encoded in the constants H_V and K_V . The mode Q_0 of the lineshape can be readily calculated from Eq. (4):

$$Q_0 \approx M_V - \frac{\Gamma_V^2 (H_V + 1) M_V}{2 [\Gamma_V^2 (H_V + K_V) - 4M_V^2]} \approx M_V + \frac{\Gamma_V^2}{8M_V} (H_V + 1), \quad (6)$$

where the approximation $\Gamma_V^2 (H_V + K_V) \ll 4M_V^2$ can be justified *a posteriori*. The quantity

$$\Delta_V \equiv \frac{\Gamma_V^2}{8M_V} (H_V + 1) \quad (7)$$

represents the displacement of the mode Q_0 from M_V . Part of it is simply due to the Jacobian factor from the transformation of Eq. (2), and does not depend on the PDFs. The right-hand side of Eq. (6) depends on K_V only at higher order in Γ_V/M_V because it enters as the coefficient of a quadratic correction to the Breit-Wigner functions, which is symmetric around M_V . Both H_V and K_V are functions of rapidity y and of the mass M_V , albeit the dependence on the latter is negligible in the range of experimental uncertainty on M_W (~ 12 MeV) and M_Z (~ 2 MeV) compared to the PDF uncertainties.

The shift Δ_V determined from Eq. (7) is plotted in Fig. 2 as a function of the boson rapidity y for W^\pm and Z production. The error bars correspond to the RMS of the distribution obtained by sampling the first 100 replicas of the chosen PDF set (NNPDF30_nlo_nf_5_pdfas from LHAPDF libraries [12]). Numerical values are reported in Table 1 for three representative values of y . It is observed a negative shift with typical size $|\Delta_V| \sim 13$ MeV in the central region $|y| \lesssim 3$, steeply increasing at larger rapidity values. This behaviour can be understood qualitatively in terms of the valence quark density xu_V and xd_V , which are typical benchmarks in PDF fits [2]. Indeed, for any derivable and positive-definite function f , it holds that

$$\frac{x f'}{f} = \frac{1}{f} (x f)' - 1. \quad (8)$$

The left-hand side of Eq. (8) is of the same form of the terms that appear in the definition of H_V (see the second line of Eq. (5)). The valence quark densities feature a local maximum at $x \sim 10^{-1}$, which corresponds to $|y| \sim 3$ at $Q \sim 90$ GeV. By identifying f in Eq. (8) with xu_V or

xd_V one can easily see that the terms $(xf)' / f$ vanish around $|y| \sim 3$, thus giving the smallest shift, whereas they steeply decrease at higher rapidity values since $f \rightarrow 0$ and $(xf)'$ becomes negative. The relative PDF uncertainty on Δ_V is found to be in the 5% ballpark, ranging from 0.3 MeV at $|y| \sim 0$ to 1 MeV at $|y| \sim 3.5$.

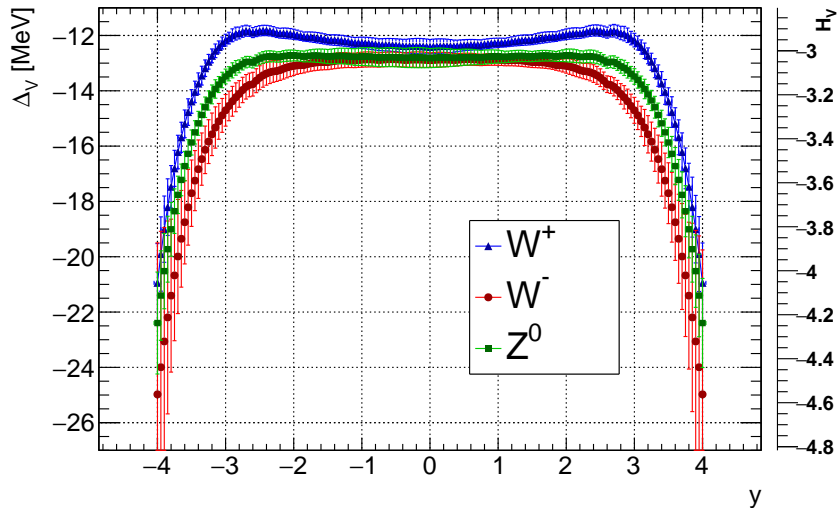


Figure 2: The shift Δ_V and the coefficient H_V as a function of y averaged over the various quark flavours that enter the tree-level production of W^\pm and Z^0 in pp collisions at $\sqrt{s} = 13$ TeV. On the right the equivalent scale for the correspondent H_V .

$ y $	W^+ [MeV]	W^- [MeV]	Z^0 [MeV]
0.0	-12.4 ± 0.3	-12.9 ± 0.3	-12.8 ± 0.3
2.0	-11.9 ± 0.2	-13.1 ± 0.3	-12.7 ± 0.2
3.5	-14.4 ± 0.5	-17.7 ± 1.1	-15.9 ± 0.5

Table 1: Numerical values of the shift Δ_V for three selected values of $|y|$ with their PDF uncertainty.

3 Monte Carlo simulation study

The tree-level calculation of Sec. 2 has been validated by using a MC simulation of $pp \rightarrow V + X$ production. Besides corroborating the tree level model, the MC analysis will also allow us to extend the study to the full phase-space, which includes the contribution of other diagrams. Given the similarity between neutral- and charged-current Drell-Yan production, and the observation that W boson production, splitted by charge, can serve as a good proxy also for the Z boson (see Fig. 2), the analysis has been restricted hereafter to the special case $V = W^\pm$. About 8×10^7 events in the final state $W^\pm \rightarrow \mu^\pm \nu_\mu$ have been generated using the MG5_aMC@NLO [13] program interfaced with Pythia8 [14]. The dilepton mass is reconstructed using the muon momentum before QED final state radiation. The MC simulation is NLO accurate for observables inclusive in extra radiation. and assumes $M_W^{\text{MC}} = 80.419$ GeV and $\Gamma_W^{\text{MC}} = 2.047$ GeV. As already anticipated in Sec. 2, it is expected to reproduce the tree-level prediction in the limit $q_T \rightarrow 0$, where q_T is the transverse momentum of the W boson. Indeed, in this regime the relative contribution of the tree-level $2 \rightarrow 1$ diagrams, which provide the unphysical spectrum $d\sigma/q_T \sim \delta(q_T)$, is enhanced compared to higher-order $2 \rightarrow 2$ diagrams. In contrast, a reduction of the shift in the large q_T

region is expected, where gluon-initiated diagrams dominate, thus reducing the sensitivity of the partonic luminosity on τ .

3.1 Fit to the MC sample

At variance with the analytical study of Sec. 2, the shift in the MC sample has to be extracted from a statistical analysis of the dilepton mass distribution $d\sigma_W^{\text{MC}}/dQ$. A crucial part of this task is to choose the correct functional form for $d\sigma_W^{\text{MC}}/dQ$, capable of modelling the lineshape without introducing a bias in the estimator of Δ_V . Motivated by the tree-level study, an *ansatz* function of the same form of Eq. (4) has been chosen:

$$\frac{d\sigma_W^{\text{MC}}}{dQ}(Q|y) = A \frac{Q^\alpha}{(Q^2 - M^2)^2 + M^2\Gamma^2} \left[1 + H \left(\frac{Q}{M} - 1 \right) + K \left(\frac{Q}{M} - 1 \right)^2 \right]. \quad (9)$$

The choice $\alpha = 1$ defines the baseline function, which it will be referred to as the *modified Breit-Wigner*. In fact, it will be explicitly validated this functional form by checking that the estimator of M_W and Γ_W is consistent with the input values of the MC simulation M_W^{MC} and Γ_W^{MC} . As a further validation of this choice, has been considered two alternative instances of the parametric family of functions in Eq. (9). The first is obtained by the choice $\alpha = H = K = 0$, which reduces to a Breit-Wigner. This function is formally incorrect to model the dilepton mass distribution since it does not account for the Jacobian factor proportional to Q . However, it is a useful benchmark since it is symmetric around $Q = M_W$, so that the mass estimator also matches the mode. The second alternative function is obtained by choosing $\alpha = 1$ and $H = K = 0$. This function, which it will be referred to as a *Breit-Wigner with Jacobian*, would be correct in the absence of the PDF distortion to the Q distribution. It peaks at $Q \approx M + \frac{\Gamma^2}{8M}$, which is always larger than M .

Three statistical analyses of the simulated events have been performed. The first analysis is inclusive in the phase-space of the W boson and allows us to benchmark the different fit functions with the largest possible statistical precision. The second analysis is differential in the W boson rapidity y and is expected to reproduce, at least qualitatively, the y -dependence from the tree-level model, as shown in Fig. 2. However, the comparison can only be approximate, since the latter predicts the transverse momentum q_T to be identically zero, whereas the MC simulation generates a physical spectrum of transverse momenta. The third analysis is performed in bins of q_T , and is inclusive in y . It allows us to both validate the tree-level calculation of Sec. 2 by extrapolating to $q_T \rightarrow 0$, and to study the dilution effect at larger values of q_T . The fit parameters of Eq. (9) are determined by minimizing a χ^2 test-statistic constructed using the event counts in each bin of the histogram in the range [79, 82] GeV and the value of the fit function at the center of the bin.

Figure 3 shows the result of the three functional fits for the inclusive analysis for W^+ sample. The W^- sample figure is omitted for brevity, but it shows very similar results. The W^- results are omitted for the same reason also for the differential analyses. The quality of the fit improves dramatically when using the modified Breit-Wigner, with a reduced χ^2 of about 1.0 compared to 1.6 and 3.9 for the alternative functions. The best-fit value of M_W when using the baseline function is consistent with the MC input within 1 ± 1 MeV, whereas the alternative functions depart from it by -9.9 ± 0.4 MeV and -21.5 ± 0.4 MeV, respectively. Likewise, the best-fit value of Γ_W is consistent with the MC input values within 1.5σ (8 ± 5 MeV) for the baseline function, while it departs from it by 18 ± 1 MeV and 16 ± 1 MeV for the alternative functions.

The best-fit value of M_W from the differential analysis in the W boson rapidity are reported in Fig. 4(a) for the W^+ sample. The Breit-Wigner fit underestimates M_W all over the rapidity

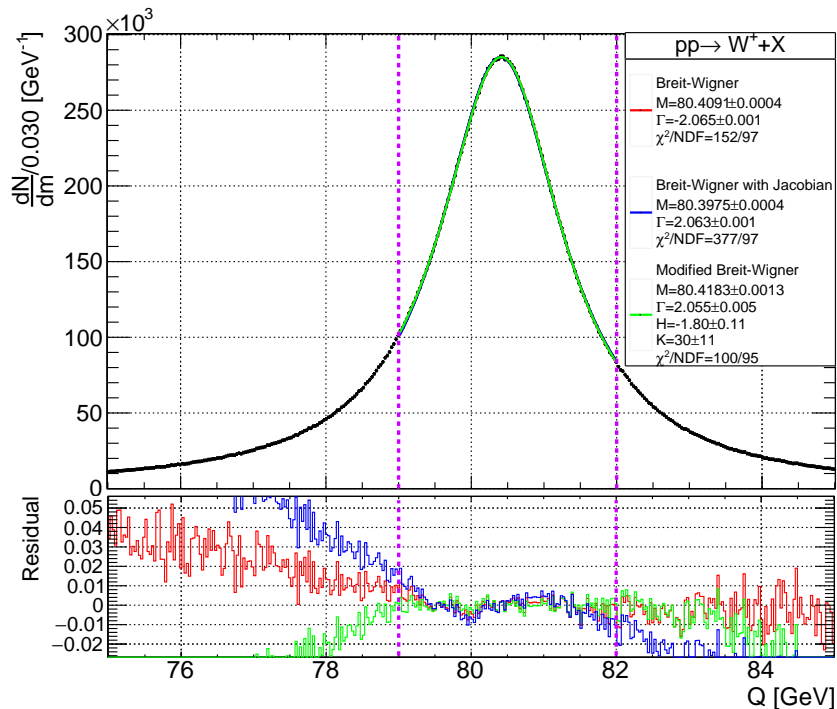


Figure 3: The dilepton mass distribution for the inclusive W^+ sample. The result of the fit using the Breit-Wigner (red), Breit-Wigner with Jacobian (blue), and modified Breit Wigner (green) are superimposed to the distributions. In the bottom pad, the residuals between the fitted function and the histogram are shown. Only events in the range [79, 82] GeV (marked by the vertical dashed lines) are used in the fit. A similar result is obtained for the W^- sample.

spectrum, as also observed in the inclusive analysis. The same applies to the Breit-Wigner with Jacobian function. For the latter, the discrepancy is even more pronounced. Indeed, the Jacobian factor contributes via a positive bias to the peak position. By neglecting the PDF term, which pulls in the opposite direction, the estimator of M_W is thus shifted to even lower values compared to M_W . The modified Breit-Wigner function correctly reproduces the input value M_W^{MC} in all bins of $|y|$, including the high $|y|$ regimes, where the alternative functions perform rather poorly. Finally, the results of the analysis differential in the W boson transverse momentum are shown in Fig. 4(b). The modified Breit-Wigner is seen to correctly reproduce the input mass value for all bins of q_T , whereas the two alternative functions disagree, especially at low transverse momenta. Above $q_T = 40$ GeV the statistical error is too large to discriminate among the models.

3.2 Extraction of Δ_W

Since the fit reproduces well the true values for M_W and Γ_W , we fix the values of M and Γ to the MC input values in Eq. 6 and repeat the fit with A, H, K as the only free parameters.

For the inclusive sample (Fig. 3) the value of the shift is found to be:

$$\begin{aligned}
 \text{(Full phase-space)} \quad \Delta_{W^+} &= -5.4 \pm 0.2 \text{ (stat.) MeV} \pm 0.1 \text{ (PDF) MeV,} \\
 \Delta_{W^-} &= -5.8 \pm 0.2 \text{ (stat.) MeV} \pm 0.1 \text{ (PDF) MeV.}
 \end{aligned} \tag{10}$$

The first uncertainty is statistical-only while the second is the estimation of the systematic uncertainty from the PDFs. The PDF uncertainty is estimated from the RMS of the shifts

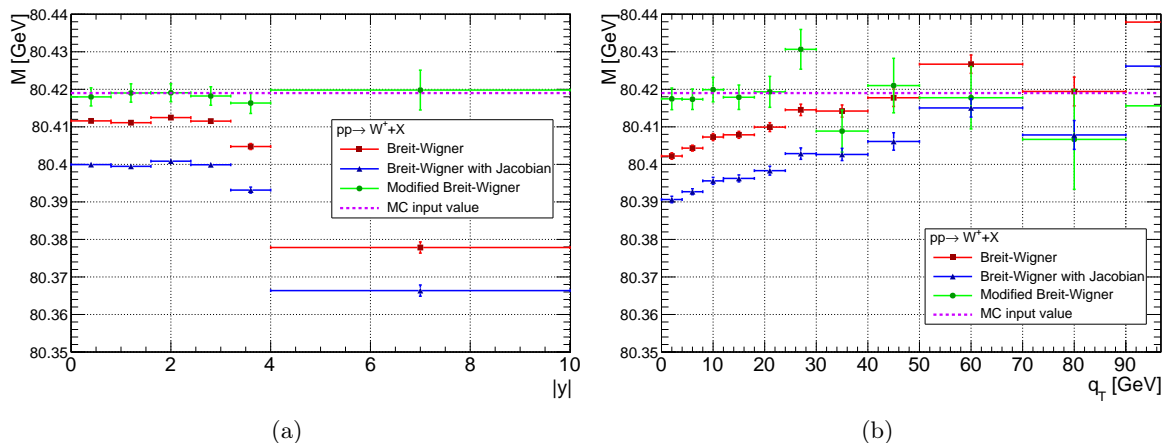


Figure 4: The best-fit value of M_W using the Breit-Wigner (red), Breit-Wigner with Jacobian (blue), and modified Breit Wigner (green), in bins of $|y|$ (left) and q_T (right), for the simulated W^+ sample. The dotted line corresponds to the input value of M_W^{MC} . A similar result is obtained for the W^- sample.

determined using the first 100 replicas, as described in Sec. 2. In these fits the parameters M and Γ have been left free, since the uncertainty on the PDFs would be otherwise over-constrained by the imposed knowledge on the mass and the width of the resonance.

The fitted values of Δ_W for the differential analyses are shown in Fig. 5 in bins of $|y|$ and q_T , separately for W^+ and W^- . The variation of Δ_W with the boson rapidity is shown in Fig. 5(a). It agrees well with the tree-level expectation of a flat shift in the central rapidity region followed by a rapid decrease at larger rapidity values. However, the shift in the central region is found to be smaller by a factor of about two, like for the inclusive results. Such difference has been interpreted as the result of the dilution from higher-order diagrams. Indeed, in the limit $q_T \rightarrow 0$, the measured shift gets closer to the tree-level result as shown by Fig. 5(b), while it vanishes for q_T in excess of about 40 GeV. A simple linear extrapolation to $q_T \rightarrow 0$ yields limiting values of

$$(q_T \rightarrow 0 \text{ extrapolation}) \quad \begin{aligned} \Delta_{W^+} &= -10.1 \pm 0.5 (\text{stat.}) \pm 0.2 (\text{PDF}) \text{ MeV}, \\ \Delta_{W^-} &= -10.0 \pm 0.6 (\text{stat.}) \pm 0.2 (\text{PDF}) \text{ MeV}. \end{aligned} \quad (11)$$

Although reasonably close to the tree-level expectation, this result still disagrees with it by roughly 30%. This residual difference is interpreted as a pure next-to-leading-order correction to the leading-order prediction, stemming from collinear gluon emission and from gluon-initiated diagrams which contribute to the small- q_T regime. The relative PDF uncertainty is found to agree reasonably well with the expectation from the tree-level model averaged over the W boson rapidity.

As a cross-check of this result, the fit after has been repeated varying the fit range symmetrically by $\pm 10\%$. The results for Δ_W are stable, with a maximum discrepancy of 5%, which is within the uncertainty of the parameter. The fit has been also repeated after changing the renormalization and factorization scales in the matrix elements of the MC simulation by factors of 0.5 and 2, respectively. The results are again found to be stable within the PDF uncertainty.

4 Conclusions

In this paper, the impact of the PDFs on the lineshape of W and Z bosons at the LHC has been investigated. Given the narrow width of the electroweak gauge bosons, the PDF impact

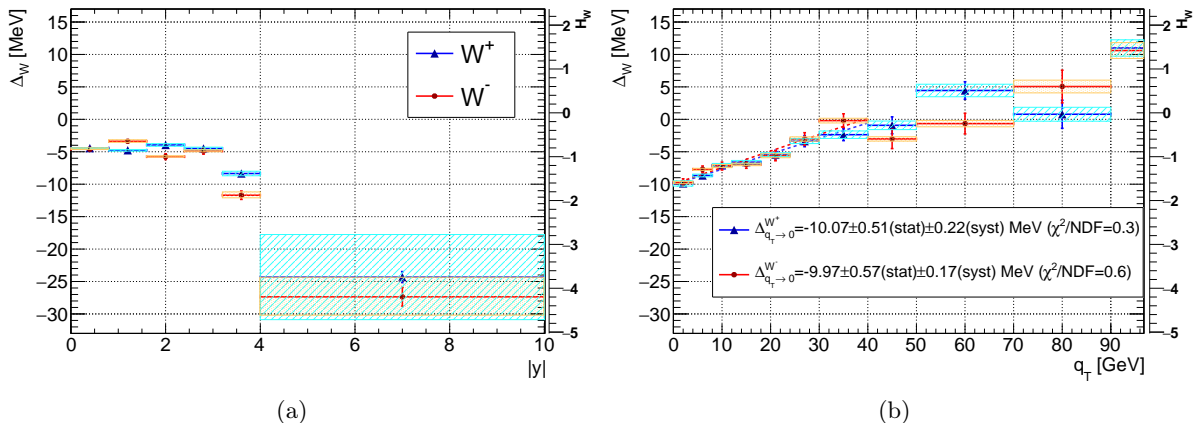


Figure 5: The shift Δ_{W^\pm} in bins of the W boson rapidity y (left) and transverse momentum q_T (right). For the latter, a linear fit in the range $[0, 40]$ MeV is performed to extrapolate the result to $q_T \rightarrow 0$. The shaded boxes correspond to the PDF systematic uncertainty, as described in the text. On the right side of each plot, the equivalent scale for the H_W parameter is reported.

can be treated, to a first approximation, as a displacement Δ_V of the mode of the dilepton mass spectrum from the boson mass M_V . The origin of such shift has been traced back to the dependence of the partonic luminosity on the virtuality Q of the gauge boson. This effect is automatically accounted for by Monte Carlo simulation of $pp \rightarrow V + X$ events. However, an uncertainty on the proton structure contributes directly to the systematic uncertainty in the extraction of M_V from the kinematics of the dilepton final state. This effect has been first studied analytically using a tree-level model of Drell-Yan production and then validated by a statistical analysis of a MC simulated sample. The tree-level calculation agrees reasonably well with the MC study in the phase-space where the two are expected to be comparable. The results of this study prove that the PDF uncertainty on Δ_V is below one MeV all over the phase space relevant for a potential mass measurement at the LHC.

References

- [1] S.D. Drell, T.M. Yan, Phys. Rev. Lett. **25**, 316 (1970). DOI 10.1103/PhysRevLett.25.316. URL <https://link.aps.org/doi/10.1103/PhysRevLett.25.316>
- [2] NNPDF collaboration, Journal of High Energy Physics **2015**(4), 40 (2015). DOI 10.1007/JHEP04(2015)040. URL [https://doi.org/10.1007/JHEP04\(2015\)040](https://doi.org/10.1007/JHEP04(2015)040)
- [3] CDF Collaboration and D0 Collaboration, Phys. Rev. D **97**, 112007 (2018). DOI 10.1103/PhysRevD.97.112007. URL <https://link.aps.org/doi/10.1103/PhysRevD.97.112007>
- [4] CMS Collaboration, The European Physical Journal C **78**(9), 701 (2018). DOI 10.1140/epjc/s10052-018-6148-7. URL <https://doi.org/10.1140/epjc/s10052-018-6148-7>
- [5] ATLAS Collaboration, Journal of High Energy Physics **2017**(12), 59 (2017). DOI 10.1007/JHEP12(2017)059. URL [https://doi.org/10.1007/JHEP12\(2017\)059](https://doi.org/10.1007/JHEP12(2017)059)
- [6] CDF Collaboration, Phys. Rev. D **89**, 072003 (2014). DOI 10.1103/PhysRevD.89.072003. URL <https://link.aps.org/doi/10.1103/PhysRevD.89.072003>

-
- [7] D0 Collaboration, Phys. Rev. D **89**, 012005 (2014). DOI 10.1103/PhysRevD.89.012005. URL <https://link.aps.org/doi/10.1103/PhysRevD.89.012005>
- [8] ATLAS Collaboration, The European Physical Journal C **78**(2), 110 (2018). DOI 10.1140/epjc/s10052-017-5475-4. URL <https://doi.org/10.1140/epjc/s10052-017-5475-4>
- [9] W.J. Stirling, A.D. Martin, Physics Letters B **237**, 551 (1990). DOI 10.1016/0370-2693(90)91223-X
- [10] R.K. Ellis, W.J. Stirling, B.R. Webber, *QCD and collider physics*. Cambridge monographs on particle physics, nuclear physics, and cosmology (Cambridge University Press, Cambridge, 2003). DOI 10.1017/CBO9780511628788. URL <https://cds.cern.ch/record/318585>
- [11] Particle Data Group, Phys. Rev. D **98**, 030001 (2018). DOI 10.1103/PhysRevD.98.030001. URL <https://link.aps.org/doi/10.1103/PhysRevD.98.030001>
- [12] A. Buckley, J. Ferrando, S. Lloyd, K. Nordström, B. Page, M. Rüfenacht, M. Schönherr, G. Watt, The European Physical Journal C **75**(3), 132 (2015). DOI 10.1140/epjc/s10052-015-3318-8. URL <https://doi.org/10.1140/epjc/s10052-015-3318-8>
- [13] J. Alwall, R. Frederix, S. Frixione, V. Hirschi, F. Maltoni, O. Mattelaer, H.S. Shao, T. Stelzer, P. Torrielli, M. Zaro, JHEP **07**, 079 (2014). DOI 10.1007/JHEP07(2014)079
- [14] T. Sjöstrand, S. Ask, J.R. Christiansen, R. Corke, N. Desai, P. Ilten, S. Mrenna, S. Prestel, C.O. Rasmussen, P.Z. Skands, Comput. Phys. Commun. **191**, 159 (2015). DOI 10.1016/j.cpc.2015.01.024